減少は介入開始後2～3年から現われ始めている[14~16]．これに対して，MIRACL試験では介入開始後約2週と早期から効果が現われ始めていることから[18]，スタチンのコレステロール依存性機序による血管壁の再構築よりも，後述するコレステロール非依存性機序の関与が推測される．

つい最近，心血管疾患あるいは高リスクの高齢者（70～82歳）を対象とし，プラバスタチン40mg/日の効果を検討するPravastatin in Elderly Individuals at Risk of Vascular Disease（PROSPER）試験の成績が報告された[19]．プラバスタチンは高齢者においても心血管疾患を19%有意に減少（P=0.006）させた．しかし，脳卒中の発症のリスクには影響を与えないことが示された．この理由として，約3年間の観察期間は脳卒中に対する有益性をみるには短かったことや検出力が十分でなかったことが指摘されている．

このように，スタチンを用いて冠動脈疾患の二次予防を目的として行われたいくつかの大規模臨床試験において，脳卒中の発症も有意に抑制されることが示されている．

一方，疫学調査の結果からスタチンを用いたTC低下療法により出血性脳卒中のリスクの増加が危惧されるが，TC低下療法に伴う出血性脳卒中の増加は認められていない[15,16,18]．

### 2）冠動脈疾患のない高コレステロール患者に対する一次予防

West of Scotland Coronary Prevention Study（WOSCOPS）研究[20]では，虚血性心疾患の既往のない中等度の高TC血症の男性を対象にプラバスタチン40mg/日の効果を検討した結果，非致死性および致死性脳卒中については11%の相対リスクの低下がみられたが，有意ではなかった（P=0.57）．冠動脈疾患を有する症例においてスタチンは脳卒中の発症予防効果がみられるが，心血管疾患のない高TC患者でのスタチンの脳卒中予防効果については評価は確立していない．

Kyushu Lipid Intervention study（KLIS）研究は，日本人男性の高TG患者を対象にプラバスタチン10～20mg/日を投与し，冠動脈疾患および脳梗塞の初発抑制効果を検討した我が国初の大規模臨床試験である[21]．プラバスタチンは，従来治療と比較して脳梗塞の相対リスクの22%の低下がみられたが，有意ではなかった（P=0.13）．本研究は，日本人の高TC血症患者においてプラバスタチンが脳梗塞の予防に有用であることを示唆する結果であった．

Japan Lipid Intervention Trial（J-LIT）研究は，冠動脈疾患や脳血管疾患の既往のない，日本人の高TC血症患者にシンバスタチン5mg/日を投与し，血清TC値と脳血管疾患の発症との関連をサブ解析で検討している．試験期間中のTC，LDL-Cが高い群ほど，ならびにHDL-Cが低い群ほど脳血管イベントの相対危険度が高く，TCでは260mg/dL以上，LDL-Cでは180mg/dL以上，またHDL-Cでは40mg/dL未満でそれぞれ有意に高かった．J-LIT研究の結果から，日本人の高TC血症患者において，TC，LDL-C高値例とHDL-C低値例では脳血管疾患のリスクが高く，脂質低下療法により血清TC値を管理することは，冠動脈疾患の予防と同様に脳血管疾患の予防に対しても効果的であることが示された．

### 3）スタチンの脳卒中予防効果に関するメタ解析

脳卒中の既往のない冠動脈疾患（二次予防）あるいは高TC血症（一次予防）を対象にしたスタチンを用いた8件の臨床試験のメタ分析では，24%（95%信頼区間，11～40%）の脳卒中の発症予防効果がみられた[22]．スタチン単独療法の臨床試験のメタ分析を行ったCrouseらの報告では，二次予防では脳卒中の相対リスクは27%の有意の低減（P=0.001）がみられたが，一次予防では脳卒中の相対リスクの低減率は15%で有意でなかった（P=0.48）[23]．スタチンを用いた13臨床試験のメタ分析では，40.4%の脳卒中の予防効果（$P<0.001$）が示されている[24]．

表 1. 脂質介入試験による脳卒中の予防効果

| 試験設定 | 試験数 | 総コレステロール | 全脳卒中数 | | オッズ比(95% CI) |
|---|---|---|---|---|---|
| | | 低下率,% (SD) | 治療群 | 対照群 | 治療/対照 |
| 一次予防 | 8 | 14.7(5.6) | 142/20,280 | 131/14,286 | 0.96(0.76-1.21) |
| 二次予防 | 25 | 18.1(6.6) | 428/14,979 | 643/18,237 | 0.80(0.71-0.91) |
| 治療 | | | | | |
| スタチン | 16 | 21.7(4.3) | 372/22,014 | 4747/17,051 | 0.77(0.67-0.87) |
| 他の薬剤 | 12 | 12.6(5.9) | 169/12,143 | 270/15,376 | 1.04(0.85-1.28) |
| 他の治療 | 5 | 14.5(3.7) | 29/1,102 | 40/1,096 | 0.72(0.44-1.17) |
| 総コレステロール低下率 | | | | | |
| < 10 % | 8 | 8.8(1.1) | 163/11,692 | 264/14,927 | 1.04(0.85-1.28) |
| 10%～20% | 13 | 15.2(3.2) | 293/12,666 | 377/12,621 | 0.77(0.66-0.90) |
| > 20 % | 12 | 23.9(3.5) | 114/10,901 | 143/5,975 | 0.75(0.59-0.96) |

(文献10より引用)

Di Mascioら[10]はスタチンを用いた16臨床試験のメタ分析を行ったところ，脳卒中のリスクの23%の有意の低減がみられた(**表 1**)．脳卒中発症のオッズ比の対数とTC低下率との回帰分析を行ったところ，TCが9%減少すると致死的および非致死的脳卒中の減少がみられることが示された．このように，スタチンを用いた冠動脈疾患の二次予防を目的として行われた臨床試験のメタ分析において，脳卒中の発症も有意に抑制されることが示されている．一方，心血管疾患のない高TC患者に対するスタチン投与(一次予防)の脳卒中発症抑制効果については評価が確立していない．

## スタチンによる脳卒中の抑制機序

スタチンはTCの低下作用のみでなく，他の作用機序から動脈硬化の進展を抑制している可能性が指摘されている．スタチンの効果は血管内皮細胞，マクロファージ，血小板，平滑筋細胞に対する作用や神経保護作用といった多面的作用(pleiotropic effect)が関与していると考えられている．

### 1．血管内皮に対する作用

高TC血症は血管内皮細胞機能を障害し，この血管内皮細胞傷害が動脈硬化の最も初期の徴候である．血管内皮機能障害の特徴は血管内皮細胞由来のnitric oxide (NO)の産生および活性の低下である．NOは動脈硬化のいくつかの過程を抑制することが知られている．そこで，NO合成酵素(NO synthethase ; NOS)の機能低下に対するスタチンの影響が検討されている．スタチンは培養血管内皮細胞のNO合成酵素(endothelial NO synthethase ; eNOS)の蛋白発現を転写後のレベルで亢進させ，それに伴ってNO産生も亢進することが示されている[25]．この作用はメバロン酸の添加によって打ち消されることから，スタチンのHMG-CoA還元酵素の阻害作用に依存する直接作用であると考えられている．

### 2．虚血性脳卒中に対する作用

スタチンの虚血性脳卒中に対する有益な効果の一部は，スタチンのeNOSの発現とその活性を亢進する作用によると考えられている[26]．虚血モデルマウスにおいてスタチンを予防的に投与すると脳血管の閉塞の後の脳血流が25～30%

表 2. 動脈硬化性疾患診療ガイドライン

| 患者カテゴリー | | | 脂質管理目標値 (mg/dL) | | | | その他の危険因子の管理 | | |
|---|---|---|---|---|---|---|---|---|---|
| | 冠動脈疾患* | 他の主要冠危険因子** | TC | LDL-C | HDL-C | TG | 高血圧 | 糖尿病 | 喫煙 |
| A | なし | 0 | <240 | <160 | ≧40 | <150 | 高血圧学会のガイドラインによる | 糖尿病学会のガイドラインによる | 禁煙 |
| B1 | | 1 | <220 | <140 | | | | | |
| B2 | | 2 | | | | | | | |
| B3 | | 3 | <200 | <120 | | | | | |
| B4 | | 4以上 | | | | | | | |
| C | あり | | <180 | <100 | | | | | |

TC：総コレステロール，LDL-C：LDLコレステロール，HDL-C：HDLコレステロール，
TG：トリグリセリド
* 冠動脈疾患とは，確定診断された心筋梗塞，狭心症とする．
** LDL-C以外の主要冠危険因子
加齢（男性≧45歳，女性≧55歳），高血圧，糖尿病，喫煙，冠動脈疾患の家族歴，低HDL-C血症（<40 mg/dL）
・ 原則としてLDL-C値で評価し，TC値は参考値とする．
・ 脂質管理は先ずライフスタイルの改善から始める．
・ 脳梗塞，閉塞性動脈硬化症の合併はB 4 扱いとする．
・ 糖尿病があれば他に危険因子がなくともB 3 とする．
・ 家族性高コレステロール血症は別に考慮する．

増加し，脳虚血病巣の大きさが50%小さくなることが示されている[26]．一方，スタチンで治療されたeNOS欠損マウスでは脳血流の増加や神経保護作用はみられなかったことから，eNOSの発現の亢進がスタチンの神経保護作用の一部を説明していると考えられている．

### 3．抗血栓作用

スタチンは線溶系の促進因子であるtissue-type plasminogen activator (t-PA) の発現を亢進し，また線溶系の抑制因子であるplasminogen activator inhibitor-1 (PAI-1) の発現を抑制することにより抗血栓作用を有することが示されている．

高TC血症はトロンボキサンA2の生合成を促進することにより，血小板機能を亢進させる．スタチンはトロンボキサンA2の産生を抑制し，血小板膜のTC含有量を低下させることにより，血小板機能を抑制することが報告されている．

### 4．抗炎症作用

動脈硬化はアテローム硬化巣へのマクロファージとTリンパ球の浸潤を特徴とする炎症機転が関与する．スタチンはアテローム硬化性プラークの炎症細胞の浸潤を抑制することによる抗炎症作用を有することが示されている．スタチンは，NO産生の亢進を介して炎症細胞の血管内皮細胞への接着に関与するP-セレクチンやintercellular adhesion molecule-1 (ICAM-1) といった接着分子の発現を抑制することが示されている．

## 脳卒中発症抑制のための治療方針

冠動脈疾患を有する高TC血症の患者では，脳卒中の発症を予防する目的でスタチンによるTC低下療法を行う．冠動脈疾患を有しない高TC血症の患者では脳卒中発症の抑制のエビデンスは現時点では明確でないので，日本動脈硬化学会による動脈硬化性疾患診療ガイドラインに準じて治療を行う（表 2）．

## 今後の展望

スタチンによる冠動脈疾患のない症例を対象としたTC低下治療における脳卒中の発症予防（一次予防）についての報告では，脳卒中の発症抑制のエビデンスは現時点では明確ではなく，今後これに関する検討が必要である．現在，国際的には冠動脈疾患の既往がなく，脳卒中またはTIAの既往のある患者に対してアトルバスタチンカルシウム水和物の投与を行い脳卒中の再発予防効果を検討する試験が進行中である（Stroke Prevention by Aggressive Reduction in Cholesterol Levels；SPARCL）．また，我が国においては厚生労働科学研究費補助金「脳血管疾患の再発に対する高脂血症治療薬のHMGCoA阻害剤の予防効果に関する研究（Japan Statin Treatment Against Reccurent Stroke, J-STARS）；主任研究者，松本昌泰」が準備中である．欧米では冠動脈疾患が多く，我が国では脳卒中が多いという特徴があり，また我が国の脳卒中の病型の特徴を考慮に入れた発症抑制に関する大規模臨床試験を行い，そのデータに基づき脳卒中の発症予防を目的とした高脂血症診療ガイドラインの作成が望まれる．

## 文　献


1) Prospective Studies Collaboration: Cholesterol, diastolic blood pressure, and stroke: 13,000 strokes in 450,000 people in 45 prospective cohorts. Lancet **346**: 1647,1995.
2) 松本昌泰，堀　正二：脳血管障害の臨床　脳血管障害発生前の危険因子とその対策　高脂血症．日本医師会雑誌 **125**: 322, 2001.
3) Iso H *et al*: Serum cholesterol levels and six-year mortality from stroke in 350, 977 men screened for the multiple risk factor intervention trial. N Engl J Med **320**: 904, 1989.
4) Benfante R *et al*: Elevated serum cholesterol is a risk factor for both coronary heart disease and thromboembolic stroke in Hawaiian Japanese men. Implications of shared risk. Stroke **25**: 814, 1994.
5) Tanaka H *et al*: Risk factors for cerebral hemorrhage and cerebral infarction in a Japanese rural community. Stroke **13**: 62, 1982.
6) Kagan A *et al*: Factors related to stroke incidence in Hawaii Japanese men. The Honolulu Heart Study. Stroke **11**: 14, 1980.
7) Lindenstrom E *et al*: Influence of total cholesterol, high density lipoprotein cholesterol, and triglycerides on risk of cerebrovascular disease: the Copenhagen City Heart Study. BMJ **309**: 11, 1994.
8) Murai A *et al*: Lipoprotein abnormalities in the pathogenesis of cerebral infarction and transient ischemic attack. Stroke **12**: 167, 1981.
9) Tanne D *et al*: Blood lipids and first-ever ischemic stroke/transient ischemic attack in the Bezafibrate Infarction Prevention (BIP) Registry: high triglycerides constitute an independent risk factor. Circulation **104**: 2892, 2001.
10) Di Mascio R *et al*: Cholesterol reduction and stroke occurrence: an overview of randomized clinical trials. Cerebrovasc Dis **10**: 85, 2000.
11) The BIP Study Group: Secondary prevention by raising HDL cholesterol and reducing triglycerides in patients with coronary artery disease: the Bezafibrate Infarction Prevention (BIP) study. Circulation **102**: 21, 2000.
12) Rubins HB *et al*: Reduction in stroke with gemfibrozil in men with coronary heart disease and low HDL cholesterol: The Veterans Affairs HDL Intervention Trial (VA-HIT). Circulation **103**: 2828, 2001.
13) Scandinavian Simvastatin Survival Study Group: Randomised trial of cholesterol lowering in 4444 patients with coronary heart disease: the Scandinavian Simvastatin Survival Study (4S). Lancet **344**: 1383, 1994.
14) Pedersen TR *et al*: Effect of simvastatin on ischemic signs and symptoms in the Scandinavian simvastatin survival study (4S). Am J Cardiol **81**: 333, 1998.
15) Plehn JF *et al*: Reduction of stroke incidence after myocardial infarction with pravastatin: the Cholesterol and Recurrent Events (CARE) study. The CARE Investigators. Circulation **99**: 216, 1999.
16) White HD *et al*: Pravastatin therapy and the risk of stroke. N Engl J Med **343**: 317, 2000.
17) Heart Protection Study Collaborative Group: MRC/BHF Heart Protection Study of cholesterol lowering with simvastatin in 20, 536 high-risk individuals: a randomised placebo-controlled trial. Lancet **360**: 7, 2002.
18) Waters DD *et al*: Effects of atorvastatin on stroke in patients with unstable angina or non-Q-wave

myocardial infarction : a Myocardial Ischemia Reduction with Aggressive Cholesterol Lowering (MIRACL) substudy. Circulation **106** :1690, 2002.
19) Shepherd J *et al* : Pravastatin in elderly individuals at risk of vascular disease (PROSPER) :a randomised controlled trial. Lancet **360** : 1623, 2002.
20) Shepherd J *et al* : Prevention of coronary heart disease with pravastatin in men with hypercholesterolemia. West of Scotland Coronary Prevention Study Group. N Engl J Med **333** : 1301, 1995.
21) The Kyushu Lipid Intervention Study Group: Pravastatin use and risk of coronary events and cerebral infarction in japanese men with moderate hypercholesterolemia : the Kyushu Lipid Intervention Study. J Atheroscler Thromb **7** : 110, 2000.
22) Bucher HC *et al* : Effect of HMGCoA reductase inhibitors on stroke. A meta-analysis of randomized, controlled trials. Ann Intern Med **128** : 89, 1998.
23) Crouse JR 3rd *et al* : Reductase inhibitor monotherapy and stroke prevention. Arch Intern Med **157** : 1305, 1997.
24) Blauw GJ *et al* : Stroke, statins, and cholesterol. A meta-analysis of randomized, placebo-controlled, double-blind trials with HMG-CoA reductase inhibitors. Stroke **28** : 946, 1997.
25) Laufs U *et al* : Upregulation of endothelial nitric oxide synthase by HMG CoA reductase inhibitors. Circulation **97** : 1129, 1998.
26) Endres M *et al* : Stroke protection by 3-hydroxy-3-methylglutaryl (HMG)-CoA reductase inhibitors mediated by endothelial nitric oxide synthase. Proc Natl Acad Sci USA **95** : 8880, 1998.

*Journal of Neurochemistry*, 2002, **81**, 497–505

# Overexpression of α7 nicotinic acetylcholine receptor prevents G1-arrest and DNA fragmentation in PC12 cells after hypoxia

Kimiaki Utsugisawa, Yuriko Nagane, Daiji Obara and Hideo Tohgi

*Department of Neurology, Iwate Medical University, Uchimaru, Morioka, Japan*

**Abstract**

We investigated the neuroprotective function of α7 nicotinic acetylcholine receptor (α7nAChR) after transient hypoxia (12 h) and reoxygenation (0–72 h), comparing rat pheochromocytoma (PC12) cells overexpressing FLAG-tagged α7nAChR (α7pCMV cells) and control PC12 cells (non-transfected or transfected with vector only) in medium with and without nicotine. Plasma membrane degradation in the early phase after hypoxia was inhibited in PC12 cells with nicotine, and more profoundly in α7pCMV cells with nicotine. Inhibition of DNA fragmentation in the late phase after hypoxia was most remarkable in α7pCMV cells with nicotine, but, surprisingly, it was more remarkable in α7pCMV cells without nicotine than in PC12 cells with nicotine. G1-arrest of the cell cycle, observed in control PC12 cells at 12 h after hypoxia, preceding DNA fragmentation, was not evident in α7pCMV cells, with or without nicotine. Furthermore, in α7pCMV cells with and without nicotine, the basal expression levels of total Akt were approximately 1.5-fold higher, and the up-regulation of Akt phosphorylated at Ser473 after hypoxia was strikingly enhanced, compared with control PC12 cells. These findings suggest that α7nAChR functions constitutively in PC12 cells, that its overexpression raises tolerance against G1-arrest and DNA fragmentation after hypoxia, and that it can be considered a candidate target for treatment against hypoxia-induced acute membrane degradation and delayed DNA fragmentation in neurons.

**Keywords:** Akt, cell cycle, G1-arrest, hypoxia, PC12, TUNEL.

*J. Neurochem.* (2002) **81**, 497–505.

Neuronal nicotinic acetylcholine receptors (nAChRs) are comprised of various combinations of α-subunits (α2–α10) and β-subunits (β2–β4) (Vijayaraghavan *et al.* 1992; Court and Clementi 1995; Breese *et al.* 1997; Elgoyhen *et al.* 2001). Functional nAChRs are classified into two principal classes according to their affinity for nicotine or α-bungarotoxin (αBTX) (Court and Clementi 1995; Breese *et al.* 1997). Of the known αBTX-binding subtypes α7–α10, only the α7 receptor has been found to be expressed throughout the mammalian brain (Vijayaraghavan *et al.* 1992; Breese *et al.* 1997; Elgoyhen *et al.* 2001). This subtype forms functional homomeric ion channels that efficiently promote $Ca^{2+}$ influx, are rapidly desensitized (Vijayaraghavan *et al.* 1992; Breese *et al.* 1997), and are assumed to modulate synaptic transmission (McGehee *et al.* 1995; Gray *et al.* 1996) and the plasticity of neuronal circuitry (Bina *et al.* 1995; Broide *et al.* 1995, 1996). Notably, nicotine reportedly exerts neuroprotective effects against cell damage due to glutamate-induced cytotoxicity and hypoxia in an αBTX-blockable manner *in vitro* (Akaike *et al.* 1994; Donnelly Roberts *et al.* 1996; Dajas-Bailador *et al.* 2000; Tohgi *et al.* 2000). Given that both agonistic stimulation and an hypoxic environment have been reported to up-regulate α7nAChR (Barrantes *et al.* 1995; Utsugisawa *et al.* 2000), this physiological cholinergic receptor may act to protect neurons from hypoxic damage and may be a promising therapeutic target. The protective effect of nicotine on cell damage is assumed to be due to $Ca^{2+}$-buffering mechanisms (Broide and Leslie 1999), agonist-mediated quick $Ca^{2+}$ currents via α7 nAChR and its rapid desensitization. However, a relatively long pre-incubation with nicotine is required for its protective effects (Akaike *et al.* 1994). Once nicotine is added to a culture medium, it prevents not only acute membrane disintegration but also DNA fragmentation approximately 24–72 h after an

Received June 18, 2001; revised manuscript received December 17, 2001; accepted January 10, 2002.

Address correspondence and reprint requests to Hideo Tohgi, Department of Neurology, Iwate Medical University, 19–1 Uchimaru, Morioka, 020–8505, Japan. E-mail: htohgi@iwate-med.ac.jp

*Abbreviations used*: αBTX, α-bungarotoxin; DMEM, Dulbecco's modified Eagle's medium; nAChRs, nicotinic acetylcholine receptors; PC12, rat pheochromocytoma cells; PI3-K, phosphatidylinositol 3-kinase; PI, propidium iodide; TUNEL, terminal deoxynucleotidyl transferase dUT nick-end labeling.

 

incidence of transient hypoxia (Tohgi *et al.* 2000). A sustained and modestly elevated intracellular $Ca^{2+}$ level may prevent cell damage (Flanklin and Johnson 1992), and nicotine exerts opposing effects on apoptosis and degeneration of neurons (according to neuronal types) via α7nAChR (Broide and Leslie 1999). Whether the various reported functions of α7nAChR are explainable simply by $Ca^{2+}$ influx remains to be determined. Recently, phosphatidylinositol 3-kinase (PI3-K) was reported to mediate neuroprotective function of α7nAChR against β-amyloid-induced cytotoxicity (Kihara *et al.* 2001).

In damaged cells, checkpoints and their related molecules in the cell cycle have an important function in selection between death and life (Yuan and Yankner 2000). Akt (protein kinase B) functions immediately downstream of PI3-K (Yuan and Yankner 2000), which targets several proteins in its role in keeping cells alive. Akt is also activated by cellular stresses including ischemia (Kitagawa *et al.* 1999; Mockridge *et al.* 2000). The rat pheochromocytoma cell line PC12 can exhibit a stable overexpression of functional α7nAChR after rat α7cDNA transfection (Cooper and Millar 1997). We investigated the neuroprotective effect of α7nAChR against hypoxia/reoxygenation in relation to changes in the cell cycle and Akt expression, comparing overexpressing PC12 cells transfected with FLAG-tagged α7cDNA (rat) and control PC12 cells (non-transfected or transfected with vector only) in medium with and without nicotine.

## Materials and methods

### Preparation of cDNA and plasmids

Full-length rat α7 subunit cDNA (Seguela *et al.* 1993) was obtained from a rat brain cDNA library (TaKaRa Bio, Otsu, Japan) by PCR using *pfu* polymerase (Promega, Madison, WI, USA). The 5′-primer of the α7 subunit was 5′-TCAAAGCTTATGTGCGGCGGGCGGGGAGGC-3′ (underline: HindIII restriction site), and the 3′-primer was 5′-GCTCTCGAGAGCAAAGTCTTTGGACACAGC-3′ (underline: *Xho*I restriction site). During α7 subunit cDNA amplification, the annealing temperature was decreased 1°C every cycle (from 69°C ) for the first 10 cycles, and was then maintained at 50°C for the following 20 cycles. The PCR products were separated electrophoretically, purified and treated with *Hind*III and *Xho*I, then inserted into the multiple cloning site of pCMV-Tag4 expression vector (C-terminal FLAG tagging vector; Stratagene, La Jolla, CA, USA) using Rapid DNA Ligation Kit$^R$ (Boehringer Mannheim, Mannheim, Germany). The transformed competent cells (Epicurian coli$^R$ XL-2 blue; Stratagene) containing ligation constructs (α7pCMV plasmid) were streaked onto LB–kanamycin–agar plates. A colony containing an accurate α7pCMV plasmid was selected by restriction analysis and full sequencing for the inserted α7 subunit cDNA using primer extension methods (TaKaRa Bio). Additionally, α7 subunit cDNA was excised from the α7pCMV plasmid at *Hind*III and *Xho*I restriction sites, bluntly treated with Klenow fragment (Gibco-BRL, Gaithersburg, MD, USA), and then inserted into an *Eco*RV site in the multiple cloning region of the pEF6/V5-His vector (C-terminal His-tagging vector; Invitrogen, Carlsbad, CA, USA) for immunoprecipitation experiments (α7pEF6 plasmid).

### Cell culture and transfection

A PC12 cell line (Greene and Tischler 1976; JCRB 0733; Human Science Research Resource Bank, Osaka, Japan) was maintained in Dulbecco's modified Eagle's medium (DMEM) supplemented with 10% fetal bovine serum (FBS), 100 units/mL penicillin, and 100 μg/mL streptomycin in a humidified atmosphere containing 5% $CO_2$ at 37°C without trypsin–EDTA for cell subculture. PC12 cells were transfected with α7pCMV plasmid using Effectene$^{TM}$ Transfection Reagent (Qiagen, Valencia, CA, USA). At the first subculture, 48 h after transfection, culture medium was supplemented with 0.75 mg/mL of G418 (Calbiochem, San Diego, CA, USA) to positively select for stable integrants (α7pCMV cells).

### Flow cytometry for estimation of the cell cycle distribution

Cells were immediately semifixed with 70% ethanol in phosphate-buffered saline (PBS), stained with propidium iodide (PI), and monitored for DNA content by FACScan (Huang *et al.* 1997). Analysis was performed for $5 \times 10^4$ cells. DNA content was assessed in order to determine the populations of G1- and G2-phase cells. The effect of αBTX on the changes resulting from of α7 subunit overexpression was studied by adding 10 μM αBTX (Molecular Probes, Eugene, OR, USA) to the medium after subculture. In our previous study, it was well enough to co-administrate 10 μM αBTX with nicotine for complete abolishment of nicotine's inhibitory effect on hypoxic neuronal damage (Tohgi *et al.* 2000).

### Induction of hypoxia

The following five subgroups were designated: untransfected PC12 cells without nicotine (control); untransfected PC12 cells with 50 μM of nicotine (PC12 cells + nicotine); PC12 cells transfected with α7pCMV plasmid, without nicotine (α7pCMV cells); α7pCMV cells with 50 μM of nicotine (α7pCMV cells + nicotine); and PC12 cells transfected with pCMV vector only (without α7cDNA), without nicotine (pCMV cells). Cells were exposed to hypoxia using a multigas incubator (Sanyo MCO, Osaka, Japan; 175 M). Briefly, after the cells were plated at a low density ($5 \times 10^4$/cm$^2$) in DMEM supplemented with 10% FBS and without G418 for 24 h in culture dishes, they were incubated in medium containing 2% FBS for 24 h, and then placed into the multi-gas incubator (2.0% $O_2$, 5% $CO_2$, balance $N_2$) at 37°C for 12 h (Yoshimura *et al.* 1998). Nicotine (Sigma, St Louis, MO, USA) was added to the medium immediately before exposure to hypoxia. In a previous study, under almost identical experimental conditions, partial oxygen pressure in the medium reportedly decreased to approximately 20 mmHg at 60 min, and then remained at this level thereafter (Goldberg *et al.* 1997). The cells were then returned to standard normoxic atmosphere for subsequent analysis at 0, 6, 12, 24, 48 and 72 h after the hypoxia (Yoshimura *et al.* 1998).

### RT-PCR and immunoblotting

For quantitation of α7 subunit mRNA, non-radioactive RT and PCR were performed as previously described (Utsugisawa *et al.* 2000).

Cell lysates were prepared in lysis buffer (50 mM HEPES, 1 mM EDTA, 150 mM NaCl, pH 7.5) containing 1% NP40, 1 mM sodium

orthovanabate (SV), 1 mM dithiothreitol (DTT), 10 mM NaF and Protein Inhibitor Cocktail (Calbiochem). Proteins were subjected to electrophoresis in sodium dodecyl sulfate (SDS)–8% polyacrylamide gel, and then transferred electrophoretically to nitrocellulose membranes (Schleicher & Schuell, Dassel, Germany). The membranes were blocked with 5% dried milk/Tris-buffered saline (pH 7.4) with 0.1% Tween-20 (TTBS), and were incubated with primary antibodies diluted 1 : 1000 for 1 h at room temperature. After washing with TTBS, the membranes were incubated with horseradish peroxidase-conjugated anti-mouse (Amersham, Piscataway, NJ, USA) or anti-rabbit IgG (Amersham) diluted 1 : 3000, and then washed with TTBS. Detection was performed using an enhanced chemiluminescence (ECL) system (NEN, Boston, MA, USA). The chemiluminescence signals from the CCD camera were integrated for 30 s, 60 s and 20 s for Akt, phosphorylated Akt and actin, respectively, into the computer memory directly from the membranes using the Chemi Doc system (BIO RAD). The density of each pixel and the number of pixels were measured and calculated. A density equal to or lower than the background was eliminated. Results were expressed as optical density × $mm^2$. Primary antibodies used were anti-total PKB/Akt (Transduction Laboratories, Lexington, KY, USA), anti-phospho-Akt (phosphorylated at Thr308 or at Ser473; New England Biolabs, Inc., Beverley, MA, USA), anti-His (Invitrogen), anti-FLAG (Sigma) and anti-actin (Progen).

### Immunoprecipitation

PC12 cells were transfected with both α7pCMV and α7pEF6 plasmids, for immunoprecipitation, to examine whether α7 subunit proteins coded for by different transfected plasmids can join to form functional receptors. Cell lysates were prepared in lysis buffer containing 0.5% NP40, 2 mM SV, 2 mM DTT, 10 mM NaF and Protein Inhibitor Cocktail. Protein lysates were incubated with anti-His or anti-FLAG antibodies at 4°C for 6 h, then with protein A- or protein G-agarose beads (Santa Cruz Biotechnology, Santa Cruz, CA, USA), respectively, at 4°C for 1 h. Beads were washed three times with lysis buffer and heated at 95°C for 5 min in reducing SDS–sample buffer. The precipitated proteins were resolved by 8% SDS–PAGE (polyacrylamide gel electrophoresis).

### Immunocytochemistry

Cells cultured in Lab-Tek$^R$ Chamber Slides$^{TM}$ (Nalge Nunc International, Naperville, IL, USA) were fixed in 4% paraformaldehyde/PBS for 5 min After the blocking procedure, the specimens were incubated with the anti-FLAG antibody (Sigma) diluted 1 : 500 in 0.5% Triton X-100/PBS (PBST) for 1 h at room temperature. After washing with PBST, they were incubated with fluorescein isothiocyanate (FITC)-conjugated anti-mouse IgG (ICN Biomedicals, East Hill, NY, USA), then washed with PBST. Immunofluorescence signals were input directly into computer memory from a Color Chilled 3CCD camera (Hamamatsu Photonics, Hamamatsu City, Japan) combined with a non-confocal fluorescence microscope (Olympus BH-2).

### Detection of plasma membrane degradation and DNA fragmentation

Cell-suspension medium was gently placed on a silan-coated slide glass, and fixed in 4% paraformaldehyde/PBS for 15 min. Propidium iodide (PI) staining and a terminal deoxynucleotidyl transferase (TdT) dUT nick-end labeling (TUNEL) method were used to detect membrane degradation and DNA fragmentation, respectively, as previously described (Tohgi *et al.* 2000). Fluorescence signals were input directly into computer memory for 5 s for PI staining and 10 s for TUNEL, under 100× magnification. The ratio of PI- and TUNEL-positive cells to total cells were determined by examining more than 500 cells.

### Statistical analysis

Where applicable, results were expressed as the mean value ± SEM of five dishes from three independent experiments. Differences of the mean for the cell groups were evaluated with Wilcoxon test for PI- and TUNEL-positive cells, and with Student's *t*-test for the expression of Akt and phospho-Akt (phosphorylated at Ser473).

## Results

### Expression of α7 subunit mRNA and α7nAChR inα7pCMV cells

The α7pCMV-positive cells selected in culture medium containing G418 (Calbiochem) over a period of 7 days, at each second day subculture, showed approximately 10-fold higher expression of FLAG-tagged α7 subunit mRNA, compared with non-transfected PC12 cells (Fig. 1a). Anti-FLAG immunocytochemistry demonstrated that α7nAChR coded for by the transfected α7 cDNA was expressed on the membranes of neurites and somata of α7pCMV cells, and that it often clustered at the hillock or the initial segments of neurites (Fig. 1b, white arrows). Immunoblotting of α7pCMV cell lysates using anti-FLAG antibody showed an approximately 55 kDa band, corresponding to the FLAG-tagged α7 subunit (Fig. 1c, smaller arrowhead). Anti-FLAG antibody detected the same approx. 55 kDa band in immunoblotting of the proteins precipitated with anti-His antibody from lysates of PC12 cells co-transfected with both α7pCMV and α7pEF6 plasmids (Fig. 1c, larger arrowhead). Anti-His antibody detected a slightly larger protein (His-tagged α7 subunit) among proteins precipitated with anti-FLAG (Fig. 1c, larger arrow); the α7 subunit coded for by the α7pEF6 plasmid had serial residues of 2 kDa at C-terminal (connected to the His tag). These results suggest that FLAG-tagged and His-tagged α7 subunit proteins form functional complexes. In our immunoprecipitation experiments, molecular sizes of both FLAG-tagged and His-tagged α7 subunit proteins were slightly smaller than that of mouse IgG heavy chain originated from primary antibodies in precipitated proteins.

### Changes in PC12 cells due to α7 overexpression

α7pCMV cells exhibited high migration ability, neurite outgrowth and adherence to the culture dish (Fig. 2a–c), but their proliferation activity, once attached firmly to the dish, was relatively low. Examination of cell cycle distribution by flow cytometry at 48 h after subculture showed relatively high

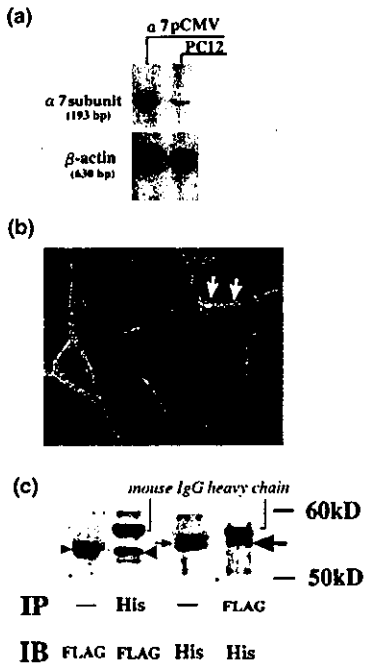


Fig. 1 Expression of α7nAChR in PC12 cells transfected with α7pCMV and α7pEF6 plasmids. (a) Quantitation of α7 subunit mRNA by non-radioactive RT-PCR. The cells stably expressing FLAG-tagged α7 subunit cDNA (α7pCMV cells) showed approximately 10-fold increase in α7 subunit mRNA, compared with non-transfected PC12 cells. (b) Anti-FLAG immunocytochemistry for α7pCMV cells. FLAG-tagged α7 subunit often clustered at the hillock or the initial segments of neurites (white arrows). Original magnification: left, × 400; right, × 1000. (c) Anti-FLAG antibody detected a band for FLAG-tagged α7 subunit in immunoblotting both of α7pCMV cell lysates (smaller arrowhead) and the proteins precipitated with anti-His antibody from lysates of PC12 cells cotransfected with α7pCMV and α7pEF6 plasmids (larger arrowhead). Anti-His antibody detected a slightly larger protein (His-tagged α7 subunit) among proteins precipitated with anti-FLAG (larger arrow). IP, immunoprecipitation; IB, immunoblotting.

G2 DNA content in α7pCMV cells, compared with PC12 cells and those transfected with pCMV vector only (Fig. 2e). The effect of α7 overexpression on high G2 DNA content were not blocked by addition of 10 μM α-bungarotoxin.

### Membrane degradation and DNA fragmentation after hypoxia

Quantitative determinations of PI-positive and TUNEL-positive cells are shown as a function of time in Fig. 3. In control PC12 cells and pCMV cells, the ratio of PI-positive cells to total cells progressively increased during and after hypoxia, reaching 34% and 32% at 72 h post-hypoxia, respectively (Fig. 3a). The increase in the ratio of PI-positive cells was inhibited most markedly in α7pCMV cells + nicotine followed by PC12 cells + nicotine, throughout the course of examination after hypoxia (Fig. 3a). In all the experimental groups, the ratio of TUNEL-positive cells to

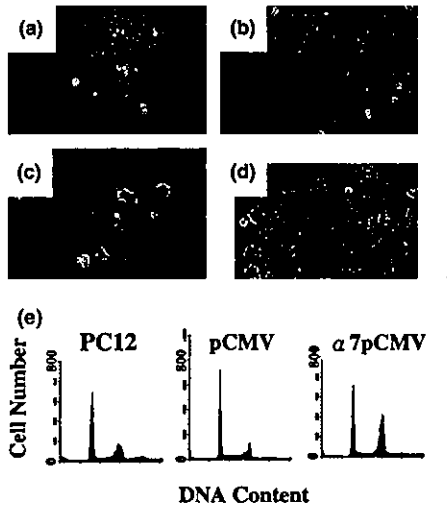


Fig. 2 Morphological changes in PC12 cells after overexpression of α7nAChR (a–c). 24 h after subculture, α7pCMV cells formed a colony (a), whereas they were observed to be dispersed 36 h after subculture (b). Seventy-two hours after subculture, α7pCMV cells grew neurites and attached firmly to the dish (c). α7pCMV cells exhibited high migration ability and neurite outgrowth. PC12 cells transfected with pCMV vector only 72 h after subculture (d). Original magnification: a,b, × 100; c,d, × 200. (e) A representative histogram of DNA content, indicating the proportion of each cell cycle phase. Flow cytometry at 48 h after subculture showed relatively high G2 DNA content in α7pCMV cells, compared with non-transfected PC12 cells and those transfected with pCMV vector only.

total cells was small (< 3%), and did not change until 12 h posthypoxia (Fig. 3b). However, in control and pCMV cells, the ratio started to progressively increase at 24 h post-hypoxia and reached 46% and 41%, respectively, at 72 h post-hypoxia (Fig. 3b). The increase in the ratio of TUNEL-positive cells was inhibited most markedly in α7pCMV cells + nicotine and, surprisingly, it was inhibited more markedly in α7pCMV cells without nicotine than in PC12 cells + nicotine throughout the course of examination after 24 h posthypoxia (Fig. 3b).

### Changes in the cell cycle after hypoxia

Representative histograms of DNA content, indicating the proportion of each cell cycle phase, for each cell line, after hypoxia, is shown in Fig. 4. In the control PC12 cells, a rise in peak representing the G1 population, which suggests G1-arrest, was observed at 12 h after hypoxia (Fig. 4, arrow), whereafter the sub-G1 population (possibly corresponding to apoptotic cells) was increased (Fig. 4). Addition of nicotine to PC12 cells postponed the onset of G1-arrest for 12 h (Fig. 4, arrowhead), but never inhibited the extent of it (Fig. 4). However, in α7pCMV cells and α7pCMV cells + nicotine, the increase in the G1 population was not observed (Fig. 4). In the control PC12 cells, tailing of G1-peak to sub-G1 also was observed at 12 h after hypoxia, which was

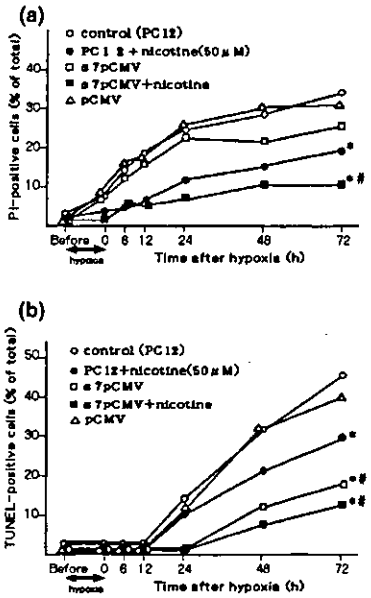


**Fig. 3** Quantitative determination of cells with membrane degradation (PI-positive; a) and DNA fragmentation (TUNEL-positive; b). (a) Increase in the ratio of PI-positive cells to total cells was inhibited most markedly in α7pCMV cells + nicotine and then in PC12 cells + nicotine throughout the course. (b) Increase in the ratio of TUNEL-positive cells to total cells was inhibited most markedly in α7pCMV cells with nicotine and, surprisingly, it was inhibited more markedly in α7pCMV cells without nicotine than in PC12 cells + nicotine throughout 24–72 h after hypoxia. Each data point represents the mean value (with SEM < 5%) of five dishes from three independent experiments. Statistical analysis were performed using Wilcoxon test. $^*p < 0.05$ compared with control PC12 cells, $\#p < 0.05$ compared with PC12 cells + nicotine at 72 h after hypoxia. ○, Control (PC12); ●, PC12 + nicotine (50 μM); □, a7pCMV; ■, a7pCMV + nicotine; △, pCMV.

prevented in other cell groups (Fig. 4). The prevention of G1-arrest in α7pCMV cells was not blocked by addition of 10 μM αBTX to the medium immediately before exposure to hypoxia. Whether more rapidly acting antagonists for nicotinic receptor than αBTX such as mecamylamine could abolish the prevention of G1-arrest remains to be determined.

### Expression and activation of Akt after hypoxia

Representative immunoblots for total Akt, phospho-Akt (phosphorylated at Ser473) and actin (as inner control) are shown in Fig. 5(a). Semi-quantitative determinations for each band of total Akt and phospho-Akt, relative to actin, are shown as a function of time in Fig. 5(b and c), respectively. In control PC12 cells, the ratio of total Akt to actin began to increase 12 h after hypoxia, and at 48 h it reached 135% of the pre-hypoxia ratio (Fig. 5b). Addition of nicotine to PC12 cells did not influence this change (Fig. 5b). However, in α7pCMV cells, with and without nicotine, the basal expression levels of total Akt were approximately 1.5-fold higher than in non-transfected PC12 cells, and remained at that level throughout the time course of the examination (Fig. 5b). In control PC12 cells, phospho-Akt was transiently up-regulated up to 24 h after hypoxia, and then began to return to the basal levels (Fig. 5c). Addition of nicotine to PC12 cells resulted in sustained up-regulation of phospho-Akt (Fig. 5c). However, in α7pCMV cells and α7pCMV cells + nicotine, the up-regulation of phospho-Akt was markedly enhanced, two-fold and three-fold immediately after hypoxia, and 1.6-fold and 2.2-fold at 6 h after hypoxia, compared with the control, respectively (Fig. 5c). These elevated phospho-Akt levels were generally maintained throughout the time course of the examination (Fig. 5c). Immunoblotting with the antibody against Akt phosphorylated at Thr308 was not able to detect this phospho-Akt (not shown).

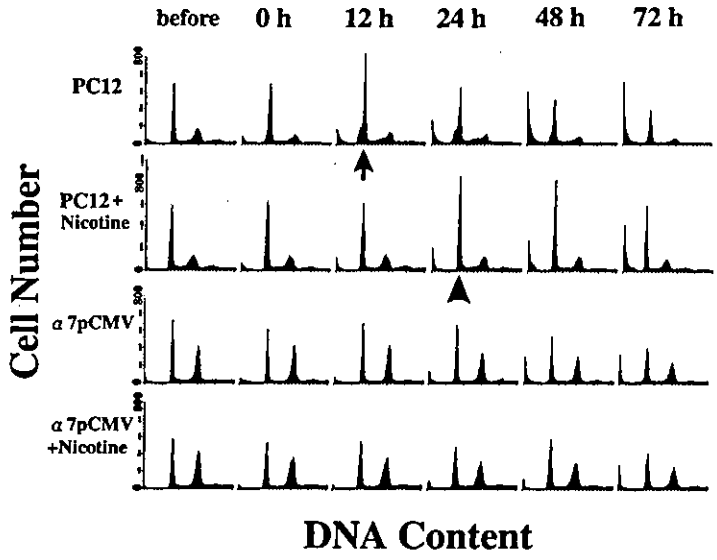


**Fig. 4** Representative histograms of DNA content, indicating the proportion of each cell cycle phase, for each cell line, after hypoxia. In the control PC12 cells, a rise in the peak representing the G1 population, which suggests G1-arrest, was observed at 12 h after hypoxia (arrow), whereafter the sub-G1 population (possibly corresponding to apoptotic cells) increased. Addition of nicotine to PC12 cells postponed the occurrence of G1-arrest for 12 h, but never inhibited (arrowhead). α7pCMV cells, with and without nicotine, did not show G1-arrest.

 

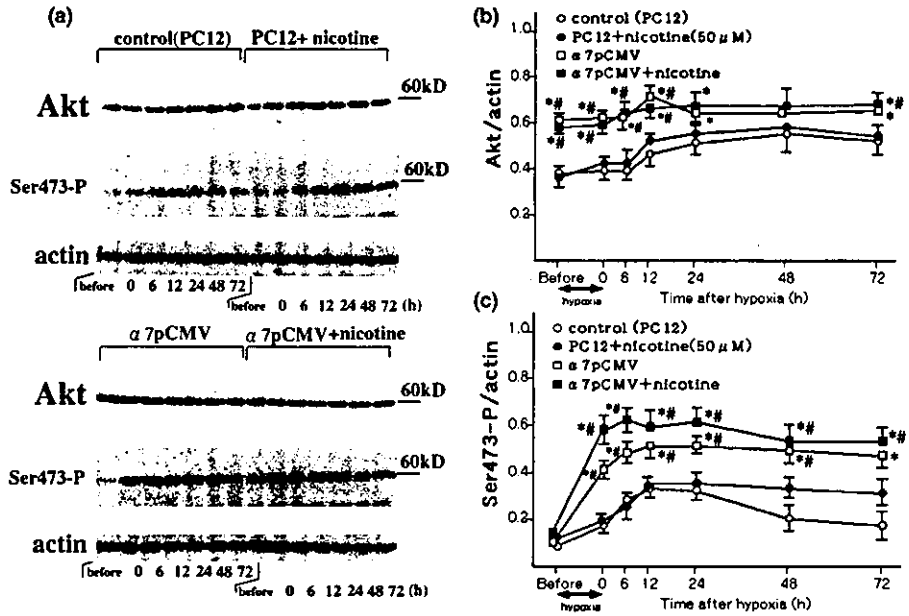


**Fig. 5** Expression of total Akt, phospho-Akt (phosphorylated at Ser473) and actin, as a function of time. (a) Representative immunoblotting. (b and c) Semi-quantitative determinations of total Akt and phospho-Akt, relative to actin, as a function of time in (b) and (c), respectively. In control PC12 cells, total Akt began to increase 12 h after hypoxia, and at 48 h it reached 135%; this was not changed by addition of nicotine (b). However, in α7pCMV cells, with and without nicotine, the basal expression levels of total Akt were approximately 1.5-fold higher than in non-transfected PC12 cells, and remained at that level throughout the time course of the examination (b). In the control PC12 cells, phospho-Akt (Ser473-P) was modestly up-regulated up to 24 h after hypoxia, and then began to return to the basal level (c). Addition of nicotine to PC12 cells resulted in sustained up-regulation of Ser473-P (c). However, in α7pCMV cells and α7pCMV cells + nicotine, there was marked up-regulation of phospho-Akt (Ser473-P), and these high levels were generally maintained throughout the course of the examination (c). Each data point represents the mean value ± SEM of five dishes from three independent experiments. Statistical analysis was performed using Student's *t*-test. $^*p < 0.05$ compared with control PC12 cells, $\#p < 0.05$ compared with PC12 cells + nicotine at the same time point. ○, Control (PC12); ●, PC12 + nicotine (50 μM); □, a7pCMV; ■, a7pCMV + nicotine.

## Discussion

The present study showed that membrane degradation was inhibited in PC12 cells with nicotine, and was inhibited even more markedly in α7pCMV cells with nicotine. The inhibititory effect of nicotine against acute membrane degradation is known to be completely blocked by αBTX (Tohgi *et al.* 2000). These findings suggest that acute membrane degradation would be prevented by an interaction between α7nAChR and its ligands. The progressive increase in DNA fragmentation seen in control PC12 and pCMV cells in the later phase of the examination (from 24 h to 72 h post-hypoxia) was inhibited most markedly in α7pCMV cells + nicotine and, surprisingly, was inhibited more markedly in α7pCMV cells without nicotine than in PC12 cells + nicotine. This finding suggests that α7 overexpression can, by itself, increase tolerability against DNA fragmentation caused by hypoxia/reoxygenation in PC12 cells. Although FLAG at C-terminal of α7 subunits is small in size (eight amino acids), the possibility that the tagging peptides may contribute to any of altered response of α7pCMV cells can not be completely ruled out. Up-regulation of α7nAChR by hypoxic environment and chronic nicotine treatment probably occurred in our experiment, which should be much less (below twofold; Barrantes *et al.* 1995; Utsugisawa *et al.* 2000) than that in α7pCMV cells (10-fold).

### Inhibition of G1-arrest in PC12 cells overexpressing α7nAChR

Apoptosis is associated with checkpoints and their related molecules in the cell cycle (Rich *et al.* 2000; Yuan and Yankner 2000). In response to hypoxia, G1-phase checkpoints are activated and p53 accumulates (Graeber *et al.* 1994; Long *et al.* 1997). In an animal model, DNA fragmentation in spinal motor neurons after transient ischemia might be associated with G1-checkpoint-related molecules (Sakurai *et al.* 2000), as is often the case with various types of cell damage (Rich *et al.* 2000). In the present study, PC12 cells exhibited an increase in G1 population, indicating G1-arrest, at 12 h post-hypoxia, before DNA fragmentation, which nicotine postponed for 12 h but did not inhibit. However, PC12 cells overexpressing α7nAChR did not exhibit G1-arrest at any time during the study, regardless of the presence/absence of nicotine. These findings suggest that

α7nAChR overexpression changes the cell cycle-regulation systems of PC12 cells, and prevents DNA fragmentation after hypoxia independently of agonistic stimulation.

### Morphological change and Akt expression in PC12 cells overexpressing α7nAChR

In the present study, a change in the expression of Akt was observed in PC12 cells overexpressing α7nAChR. Akt is activated by cellular stresses including ischemia (Kitagawa *et al.* 1999; Mockridge *et al.* 2000), and keeps neurons alive by various mechanisms (Yuan and Yankner 2000). In control PC12 cells and PC12 cells + nicotine, total Akt modestly increased from 12 to 48 h after post-hypoxia. However, in cells overexpressing α7, the basal expression level of total Akt was approximately 1.5-fold higher than in non-transfected PC12 cells, and this high level was maintained throughout the experiment. It has been reported that Akt expression was low in a particular multipotent cell line, but increased with differentiation into myocytes with MyoD (Coffer *et al.* 1998) and, conversely, that 3T3-L1 fibroblasts differentiate into adipocytes when transfected with Akt (Coffer *et al.* 1998). Thus, expression of Akt appears to be tightly connected to differentiation in various cell types (Coffer *et al.* 1998). The high migration ability, neurite outgrowth, and adherence of α7pCMV cells observed in the present study are similar to the characteristics of PC12 cells differentiated with nerve growth factor (NGF). α7nAChR-specific machinery for successful folding and multimeric expression after transfection seems to involve cytoskeletal architecture and specific molecular interaction to the receptor (Blumenthal *et al.* 1997; Cooper and Millar 1997; Shoop *et al.* 2000). The spontaneous expression of α7nAChR in PC12 cells also differs according to their relative adherence, morphology (Utsugisawa *et al.* 2000), and NGF-induced differentiation (Takahashi *et al.* 1999). Therefore, overexpression of α7nAChR may be connected with cytoskeletal architecture and function, promoting a differentiation-like transformation which may influence Akt regulation. Moreover, a morphogenesis checkpoint in the cell cycle, in which actin organization is directly monitored, delays nuclear division and possibly increases the G2 population (McMillan *et al.* 1998), and may be related to a rise in the G2 population at steady state observed in α7pCMV cells.

### Up-regulation of phospho-Akt in PC12 cells overexpressing α7 nAChR

In the present study, in the controls, Akt phosphorylated at Ser473 (phospho-Akt) was transiently up-regulated until 24 h after hypoxia, and then returned to the basal level. The transient up-regulation of phospho-Akt has also been shown in ischemic rat hippocampus (Ouyang *et al.* 1999) and myocytes (Mockridge *et al.* 2000). In the presence of nicotine, this up-regulation of phospho-Akt was sustained up to 72 h after hypoxia. Furthermore, in α7pCMV cells, with and without nicotine, the up-regulation of phospho-Akt was markedly enhanced, and was generally maintained throughout the course of the examination. Because phospho-Akt can promote the cell cycle by activation of p70 S6 kinase (Kitamura *et al.* 1998; Zhong *et al.* 2000), Akt activation in the present study might also have inhibited or postponed G1-arrest in α7-overexpressing or nicotine-added PC12 cells, and promoted cell survival.

The enhanced phosphorylation of Akt in cells overexpressing α7nAChR may be in part explained by the increase in the basal level of total Akt. However, immunoblotting with an antibody against Akt phosphorylated at Thr308 failed to detect phospho-Akt. Upon stimulation of PI3-K activity, Akt becomes phosphorylated at two residues, Thr308 and Ser473, both of which are required for full activation (Coffer *et al.* 1998). While activation of PI3-K appears to induce Akt activation universally, it is not the only mechanism of Akt activation. For example, heat-shock-mediated activation of Akt is insensitive to inhibition of PI3-K (Coffer *et al.* 1998). The mutational analysis of Thr308 and/or Ser473 suggests that the two sites are independently regulated (Alessi *et al.* 1996; Coffer *et al.* 1998). The phosphorylation mechanisms for Ser473 site after hypoxic cell damage remains to be investigated.

In conclusion, α7nAChR overexpression increases tolerance against G1-arrest and DNA fragmentation, along with changes in Akt expression, in PC12 cells after hypoxia. Given that certain types of neuronal receptors reportedly show constitutive activity without ligands (Morisset *et al.* 2000), overexpressed α7nAChR may also affect cellular machinery, details of which remain to be determined. Because the patterns of inhibition of plasma membrane degradation and DNA fragmentation were different, and rather independent of each other, these processes should be individually targeted in attempts to rescue neurons from damage after hypoxia. Although PC12 cells differ somewhat from mature neurons in the human brain, the present study provides further evidence that α7nAChR could be a candidate target for treatment against hypoxia-induced acute membrane degradation and delayed DNA fragmentation in neurons.

## Acknowledgements

We wish to thank Dr Taiju Utsugisawa for his technical advice and Ms Sakuyo Nagai for her technical assistance. This study was supported in part by the Ministry of Education, Culture, Sports, Science and Technology, Japan.

## References

Akaike A., Tamura Y., Yokota T., Shimohama S. and Kimura J. (1994) Nicotine-induced protection of cultured cortical neurons against *N*-methyl-D-aspartate receptor-mediated glutamate cytotoxicity. *Brain Res.* **644**, 181–187.

Alessi D. R., Andjelkovic M., Caudwell B., Cron P., Morrice N., Cohen P. and Hemmings B. A. (1996) Mechanism of activation of protein kinase B by insulin and IGF-1. *EMBO* **15**, 6541–6551.

Barrantes G. E., Rogers A. T., Lindstrom J. and Wonnacott S. (1995) a-bungarotoxin binding sites in rat hippocampal and cortical cultures: initial characterization, co-localization with α7 subunits and up-regulation by chronic nicotine treatment. *Brain Res.* **672**, 228–236.

Bina K. G., Guzman P., Broide R. S., Leslie F. M., Smith M. A. and O'Dowd D. K. (1995). Localization of α7 nicotinic receptor subunit mRNA and α-bungarotoxin binding sites in developing mouse somatosensory thalamocortical system. *J. Comp. Neurol.* **363**, 321–332.

Blumenthal E. M., Conroy W. G., Romano S. J., Kassner P. D. and Berg D. K. (1997) Detection of functional nicotinic receptors blocked by α-bungarotoxin on PC12 cells and dependence of their expression on post-translational events. *J. Neurosci.* **17**, 6094–6104.

Breese C. R., Adams C., Logel J., Drebing C., Rollins Y., Barnhart M., Sullivan B., . Demasters B. K., Freedman R. and Leonard S. (1997) Comparison of the regional expression of nicotinic acetylcholine receptor α7 mRNA and [$^{125}$I]-α-bungarotoxin binding in human postmortem brain. *J. Comp. Neurol.* **387**, 385–398.

Broide R. S. and Leslie F. M. (1999) The α7 nicotinic acetylcholine receptor in neuronal plasticity. *Mol. Neurobiol.* **20**, 1–16.

Broide R. S., O'Connor L. T., Smith M. A., Smith J. A. M. and Leslie F. M. (1995) Developmental expression of α7 neuronal nicotinic receptor messenger RNA in rat sensory cortex and thalamus. *Neuroscience* **67**, 83–94.

Broide R. S., Robertson R. T. and Leslie F. M. (1996) Regulation ofa7 nicotinic acetylcholine receptors in the developing rat somatosensory cortex by thalamocortical afferents. *J. Neurosci.* **16**, 2956–2971.

Coffer P. J., Jin J. and Woodgett J. R. (1998) Protein kinase B (c-Akt): a multifunctional mediator of phosphatidylinositol 3-kinase activation. *Biochem. J.* **335**, 1–13.

Cooper S. T. and Millar N. S. (1997) Host cell-specific folding and assembly of the neuronal nicotinic acetylcholine receptor α7 subunit. *J. Neurochem.* **68**, 2140–2151.

Court J. and Clementi F. (1995) Distribution of nicotinic subtypes in human brain. *Alz. Dis. Assoc. Dis.* **9**, 6–14.

Dajas-Bailador F. A., Lima P. A. and Wonnacott S. (2000) The α7 nicotinic acetylcholine receptor subtype mediates nicotine protection against NMDA excitotoxicity in primary hippocampal cultures through a $Ca^{2+}$ dependent mechanism. *Neuropharmacology* **39**, 2799–2807.

Donnelly-Roberts D. L., Xue I. C., Arneric S. P. and Sullivan J. P. (1996) *In vitro* neuroprotective properties of the novel cholinergic channel activator (ChCA), ABT-418. *Brain Res.* **719**, 36–44.

Elgoyhen A. B., Vetter D. E., Katz E., Rothlin C. V., Heinemann S. F. and Boulter J. (2001) α10: a determinant of nicotinic cholinergic receptor function in mammalian vestibular and cochlear mechanosensory hair cells. *Proc. Natl. Acad. Sci. USA* **98**, 3501–3506.

Flanklin J. I. and Johnson E. M. Jr (1992) Suppression of programmed neuronal death by sustained elevation of cytoplasmic calcium. *Trends Neurosci.* **15**, 501–508.

Goldberg M., Zhang H. L. and Steinberg S. F. (1997) Hypoxia alters the subcellular distribution of protein kinase C isoforms in neonatal rat ventricular myocytes. *J. Clin. Invest.* **99**, 55–61.

Graeber T. G., Peterson J. F., Tsai M., Monica S., Fornace A. J. Jr and Giaccia A. (1994) Hypoxia induces accumulation of p53 protein, but activation of a G1-phase checkpoint by low-oxygen conditions is independent of p53 status. *Mol. Cell. Biol.* **14**, 6264–6277.

Gray R., Rajan A. S., Radcliffe K. A., Yakehiro M. and Dani J. A. (1996) Hippocampal synaptic transmission enhanced by low concentrations of nicotine. *Nature* **383**, 713–716.

Greene L. A. and Tischler A. S. (1976) Establishment of a noradrenergic clonal line of rat adrenal pheochromocytoma cells which respond to nerve growth factor. *Proc. Natl. Acad. Sci. USA* **73**, 2424–2428.

Huang Y., Yuan Z.-M., Ishiko T., Nakada S., Utsugisawa T., Kato T., Kharbanda S. and Kufe D. W. (1997) Pro-apoptotic effect of the c-Abl tyrosine kinase in the cellular response to 1-β-D-arabinofuranosylcytosine. *Oncogene* **15**, 1947–1952.

Kihara T., Shimohama S., Sawada H., Honda K., Nakamizo T., Shibasaki H., Kume T. and Akaike A. (2001) α7 nicotinic receptor transduces signals to phosphatidylinositol 3-kinase to block Aβ-amyloid-induced neurotoxicity. *J. Biol. Chem.* **276**, 13541–13546.

Kitagawa H., Warita H., Sasaki C., Zhang W. R., Sakai K., Shiro Y., Mitsumoto Y., Mori T. and Abe K. (1999) Immunoreactive Akt, PI3-K and ERK protein kinase expression in ischemic rat brain. *Neurosci. Lett.* **274**, 45–48.

Kitamura T., Ogawa W., Sakaue H., Hino Y., Kuroda S., Takata M., Matsumoto M., Maeda T., Konishi H., Kikkawa U. and Kasuga M. (1998) Requirement for activation of the serine–threonine kinase Akt (protein kinase B) in insulin stimulation of protein synthesis but not of glucose transport. *Mol. Cell. Biol.* **18**, 3708–3717.

Long X., Boluyt M. O., Hipolito M., Lundberg M. S., Zheng J.-S., O'Nell L., Cirielli C., Lakatta E. G. and Crow M. T. (1997) p53 and the hypoxia-induced apoptosis of cultured neonatal rat cardiac myocytes. *J. Clin. Invest.* **99**, 2635–2643.

McGehee D. S., Heath M. J. S., Gelber S., Devay P. and Role L. W. (1995) Nicotine enhancement of fast excitatory synaptic transmission in CNS by pre-synaptic receptors. *Science.* **269**, 1692–1696.

McMillan J. N., Sia R. A. L. and Lew D. J. (1998) A morphogenesis checkpoint monitors the actin cytoskeleton in yeast. *J. Cell Biol.* **142**, 1487–1499.

Mockridge J. W., Marber M. S. and Heads R. J. (2000) Activation of Akt during simulated ischemia/reperfusion in cardiac myocytes. *Biochem. Biophys. Res. Commun.* **270**, 947–952.

Morisset S., Rouleau A., Ligneau X., Gbahou F., Tardivel-Lacombe J., Stark H., Schunack W., Ganellin C. R., Schwartz J.-C. and Arrang J.-M. (2000) High constitutive activity of native $H_3$ receptors regulates histamine neurons in brain. *Nature* **408**, 860–864.

Ouyang Y.-B., Tan Y., Comb M., Liu C.-L., Martone M. E., Siesjo B. K. and Hu B.-R. (1999) Survival- and death-promoting events after transient cerebral ischemia: phosphorylation of Akt, release of cytochrome C, and activation of caspase-like proteases. *J. Cereb. Blood Flow Metab.* **19**, 1126–1135.

Rich T., Allen R. L. and Wyllie A. H. (2000) Defying death after DNA damage. *Nature.* **407**, 777–783.

Sakurai M., Hayashi T., Abe K., Itoyama Y. and Tabayashi K. (2000) Cyclin D1 and Cdk4 protein induction in motor neurons after transient spinal cord ischemia in rabbits. *Stroke* **31**, 200–207.

Seguela P., Wadiche J., Dineley-Miller K., Dani J. A. and Patrick J. W. (1993) Molecular cloning, functional properties, and distribution of rat brain α7: a nicotinic cation channel highly permeable to calcium. *J. Neurosci.* **13**, 596–604.

Shoop R. D., Yamada N. and Berg D. K. (2000) Cytoskeletal links of neuronal acetylcholine receptors containing α7 subunits. *J. Neurosci.* **20**, 4021–4029.

Takahashi T., Yamashita H., Nakamura S., Ishiguro H., Nagatsu T. and Kawakami H. (1999) Effects of nerve growth factor and nicotine

on the expression of nicotinic acetylcholine receptor subunits in PC12 cells. *Neurosci. Res.* **35**, 175–181.

Tohgi H., Utsugisawa K. and Nagane Y. (2000) Protective effect of nicotine through nicotinic acetylcholine receptor α7 on hypoxia-induced membrane disintegration and DNA fragmentation of cultured PC12 cells. *Neurosci. Lett.* **285**, 91–94.

Utsugisawa K., Nagane Y., Obara D. and Tohgi H. (2000) Increased expression of α7 nAChR after transient hypoxia in PC12 cells. *Neuroreport* **11**, 2209–2212.

Vijayaraghavan S., Puch P. C., Zhang Z. W., Rathouz M. M. and Berg D. K. (1992) Nicotinic receptors that bind α-bungarotoxin on neurons raise intracellular free $Ca^{2+}$. *Neuron* **8**, 353–362.

Yoshimura S., Banno Y., Nakashima S., Takenaka K., Sakai H., Nishimura Y., Sakai N., Shimizu S., Eguchi Y., Tsujimoto Y. and Nozawa Y. (1998) Ceramide formation leads to caspase-3 activation during hypoxic PC12 cell death. *J. Biol. Chem.* **273**, 6921–6927.

Yuan J. and Yankner B. A. (2000) Apoptosis in the nervous system. *Nature* **407**, 802–809.

Zhong H., Chiles K., Feldser D., Laughner E., Hanrahan C., Georgescu M.-M., Simons J. W. and Semenza G. L. (2000) Modulation of hypoxia-inducible factor 1a expression by the epidermal growth factor/phosphatidylinositol 3-kinase/PTEN/AKT/FRAP pathway in human prostase cancer cells: implications for tumor angiogenesis and therapeutics. *Cancer Res.* **60**, 1541–1545.

ELSEVIER

Neuroscience Letters 332 (2002) 45–48

Neuroscience Letters

www.elsevier.com/locate/neulet

# Selective reduction of diffusion anisotropy in white matter of Alzheimer disease brains measured by 3.0 Tesla magnetic resonance imaging

Satoshi Takahashi[a], Hisashi Yonezawa[a], Junko Takahashi[a], Masako Kudo[a], Takashi Inoue[b], Hideo Tohgi[a,*]

[a]Department of Neurology, Iwate Medical University, Morioka, Iwate, Japan
[b]Department of Neurosurgery, Iwate Medical University, Morioka, Iwate, Japan

Received 26 July 2002; received in revised form 10 August 2002; accepted 12 August 2002

**Abstract**

Alzheimer disease (AD) is pathologically characterized by cortical atrophy. Changes in the white matter and their relation to the pathogenesis of AD remain to be studied. To quantitatively investigate the integrity and organization of white matter fiber tracts in patients with AD, we used diffusion tensor (DT) imaging to study the diffusion anisotropy of white matter regions. DT imaging was performed using a 3.0 Tesla magnetic resonance scanner in ten probable AD patients with no or only mild changes in the white matter in T2 weighted magnetic resonance imagings and ten group-matched controls. The values of fractional anisotropy were significantly lower in the temporal subcortical white matter, posterior part of the corpus callosum, and anterior and posterior cingulate bundles in patients with AD compared with controls. Possible relationships of these selective impairments in the white matter with pathological changes in the poterior cerebral cortices and hippocampus were discussed. 

*Keywords*: Alzheimer disease; White matter; Diffusion tensor imaging; 3.0 Tesla magnetic resonance imaging (magnetic resonance imaging)

Alzheimer disease (AD) is pathologically characterized by degeneration and atrophy of the cerebral cortex. Although mild changes of the subcortical white matter such as leukoaraiosis are seen in some cases [8,10,13], whether they are simply a manifestation of concomitant vascular dementia or are related to the pathogenesis of AD is undertermined. Previous studies using conventional magnetic resonance (MR) imaging or evaluation of autopsy brains have reported the reduction in the size of the corpus callosum in AD, although regional differences in the degree of atrophy have been controversial [4,26,27]. Conventional MR imaging has limited capability to quantitate changes in the subcortical white matter.

The integrity of nerve fiber tracts can be investigated by evaluating diffusion anisotropy. Diffusion-weighted MR imaging visualizes movements of water molecules within tissues [22]. The movement of water molecules in tissues is not Brownian, but has a direction determined by many factors including cell membranes, axonal membranes, and cytoskeletal structures such as neurofilaments and microtubules [3]. As such anisotropic movements of water particularly dominate in regions enriched with axons, quantitative measurement of diffusion anisotropy determined by diffusion tensor (DT) analysis can be an indicator of the integrity of the cerebral white matter. Previous studies using 1.5 Tesla MR imaging have reported a decrease in anisotropy in a few areas of the white matter of patients with AD [5,6,21]. The purpose of this study was to investigate changes in the diffusion anisotropy in nine areas of white matter fiber tracts in patients with probable AD using 3.0 Tesla MR imaging, which, compared with 1.5 Tesla MR imaging, allows much more accurate quantitation of anisotropy in smaller regions with a relatively low coherence of fiber direction.

Subjects were ten patients with probable AD (three males and seven females; 70 ± 4 years old, mean ± SD; range, 5286) and ten control subjects (two males and eight females; 70 ± 10 years old; range, 6576). The diagnosis of AD was made according to the criteria of NINCDS-ADRDA [16]. In

* Corresponding author. Iwate Medical University, 19-1 Uchimaru, Morioka, Iwate 020-8505, Japan. Fax: +81-19-654-9860.
*E-mail address:* htohgi@iwate-med.ac.jp (H. Tohgi).

0304-3940/02/$ - see front matter 
PII: S0304-3940(02)00914-X

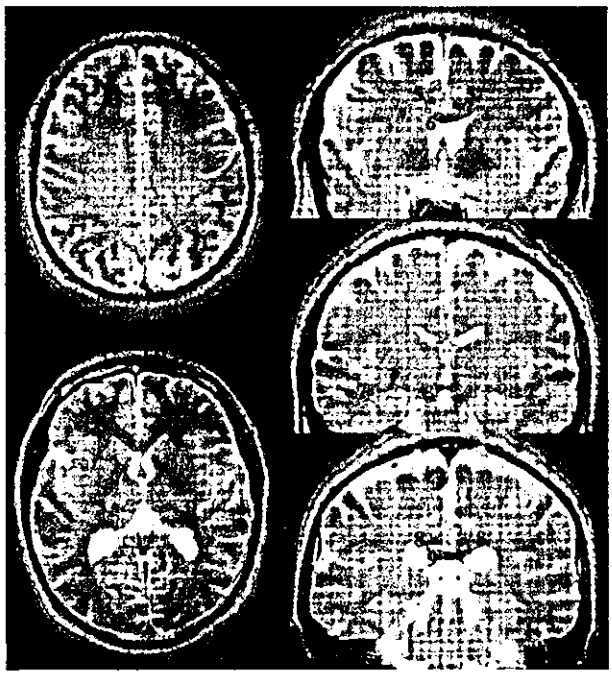

Fig. 1. Location of ROIs as shown in the horizontal (left) and frontal (right) planes. 1, subcortical white matter (SWM) in the parietal lobe; 2, SWM in the frontal lobe; 3, internal capsule; 4, SWM in the occipital lobe; 5, anterior cingulum; 6, anterior portion of corpus callosum; 7, SWM in the temporal lobe; 8, posterior cingulum; 9, posterior portion of corpus callosum.

the patients with AD, the disease duration was 3.8 ± 1.3 years (range, 26) and the minimental state examination (MMSE) score [12] was 19.0 ± 3.2 (range: 1423); four patients were at Stage 4 and six at Stage 5 according to Functional Assessment Staging [19]. T2 weighted MR imagings in the patients with AD showed very mild white matter changes (Fazekas' Grade 1) in two cases and no changes (Fazekas' Grade 0) in the other eight cases [11]. Control subjects were neurologically normal volunteers whose T2 weighted MR imagings were normal. Informed consent was obtained from all the subjects.

All scans were performed using a Signa VH/i 3.0 T MR imaging system (GE Medical Systems, Milwaukee, WI) and a standard head coil. Prior to DT imaging, all patients underwent conventional spin echo proton density-weighted and T2 weighted MR imaging: repetition time (TR) 2800 ms, echo time (TE) 30 ms or 100 ms, matrix 512 × 320, field of view (FOV) 220 × 220 mm, 3 mm thickness, and 1 mm gap. A spin echo type echo planar imaging sequence with diffusion gradients applied in six directions was used for DT imaging (TR 3000 ms, TE 84 ms, matrix 128 × 128, FOV 240 × 180 mm, 6 mm thickness, and 2 mm gap. To optimize the measurement of diffusion, only two b factors were used (b1 = 0, b2 = 1200 s/mm$^2$).

All images were post-processed on a workstation (Ultra 2; Sun Microsystems, Mountain View, CA) connected to the scanner, using a subprogram of the Functoll$^{TM}$ image analysis software (General Electric Medical Systems, Buc, France). The scalars in variants of the tensor, including the eigenvalues $\lambda_1$, $\lambda_2$, and $\lambda_3$ were derived for every pixel. As the index of the degree of anisotropy, we used fractional anisotropy (FA, dimensionless, 0.0–1.0) [2], which is defined as

$$\mathrm{FA} = \sqrt{\frac{3}{2}}\frac{\sqrt{(\lambda_1 - <D>)^2 + (\lambda_2 - <D>)^2 + (\lambda_3 - <D>)^2}}{\sqrt{\lambda_1^2 + \lambda_2^2 + \lambda_3^2}}$$

where $<D>$ is the average of the trace of the diffusion tensor $D$.

$$<D> = \frac{1}{3}\mathrm{Tr}(D) = \frac{1}{3}\left(\lambda_1^2 + \lambda_2^2 + \lambda_3^2\right)$$

The regions of interest (ROI, round areas of 25 mm$^2$) were the subcortical white matter fiber tracts in the middle frontal gyrus (frontal), angular gyrus (parietal), occipital apex (occipital), and the internal capsule in the axial slices, and the anterior (at the plane of the optic chiasm) and posterior (at the plane of the anterior part of the inferior colliculus) portions of the corpus callosum and the cingulate bundle in the coronal slices (Fig. 1). For symmetrically located ROIs, the average FA value of corresponding right and left ROIs was taken for individual regions. Statistical analysis was performed using Mann–Whitney $U$-test. The alpha level for statistical significance was established at 0.05.

The FA values in controls differed among ROIs, ranging from about 0.2 (in subcortical white matter) to 0.4–0.7 (in the internal capsule and corpus callosum), depending upon the degree of coherence of fiber tract direction. Compared with controls, the FA value in patients with AD was significantly reduced in the temporal lobe white matter, anterior and posterior cingulate bundles, and posterior portion of the corpus callosum ($P < 0.05$, Fig. 2). The FA values were lower in patients with AD than in controls in the parietal, temporal, and occipital subcortical regions, and the reduction in the FA value was significant in the temporal regions. The difference was most remarkable in the posterior cingulate bundles (~33% of controls, $P < 0.005$, Fig. 3). For each area studied, the reduction in the FA value was not corre-

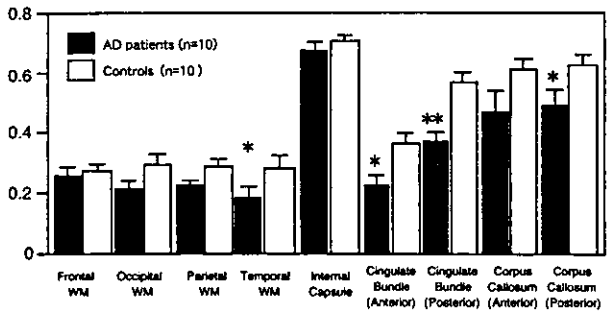


Fig. 2. Regional FA values in patients with Alzheimer disease (filled columns) and controls (open columns). Mean ± SE. *P < 0.05, **P < 0.005 compared with controls (Mann–Whitney $U$-test).

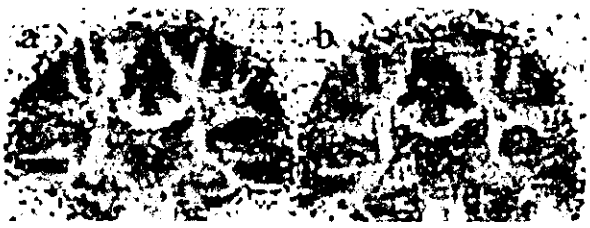


Fig. 3. Representative FA images in a frontal plane cut through the posterior cingulum (arrow heads) in a control (a) and in a patient with Alzheimer disease (b).

lated with MMSE scores (14–23) in these mild to moderate cases of AD.

The present study demonstrated significant reductions in the FA values in selected areas, including the temporal white matter, posterior portion of the corpus callosum, and anterior and posterior portions of the cingulate bundles in patients with AD. The reduction in the FA values suggests a reduction in axon number, an impairment of axonal flow, or both. As the present AD patients had no or only mild changes on T1 and T2 MR imagings, the findings may likely represent white matter changes caused purely by AD pathology, excluding those possibly related to hypoperfusion caused by amyloid angiopathy [8] or concomitant vascular dementia. The findings suggest that DT imaging appears much more sensitive to the disintegration of neuronal fibers than are pathological observation or conventional MR imaging.

The significant reduction in the FA values in the temporal subcortical white matter and the posterior portion of the corpus callosum may reflect the pathologically proven distribution of neurofibrillary tangles and senile plaques in the cerebral cortex. These pathological landmarks of AD are more prevalent in the posterior brain and in the temporal and parietal association cortices than in the anterior brain [1]. Neurofibillary tangles predominate in entorhinal cortex layers II and IV and in association cortex layers II, III and V; the neurofibrillary tangle-bearing cells are large pyramidal projection neurons [18,20] and are primarily glutamatergic [15]. The presence of neurofibrillary tangles may cause or reflect degeneration of projection fibers in the white matter and impaired cortico-cortical and cortico-subcortical connections [23].

Although atrophy of the corpus callosum is macroscopically evident in autopsy cases in the advanced phase, it can only be evaluated by neuroimaging studies in mild cases. The present results regarding the corpus callosum are consistent with some previous reports using conventional MR imaging [4,27] or analysis with diffusion anisotropy [14]. Hanyu et al. reported that the fractional isotropy (FI) value, the inverse of the fractional anisotropy, was increased in both the anterior and the posterior portions of the corpus callosum, but that the change was much more remarkable in the posterior corpus callosum [14]. The disintegration of primarily the posterior corpus callosum suggests that this portion of the corpus callosum, which interconnects temporal, parietal, and occipital cortices, may have been affected secondarily to cortical degeneration in AD.

A particularly important finding in the present study is the most remarkable reduction of FA in the posterior cingulate bundles of patients with AD. Rose et al. have also reported the reduction in a measure of anisotropy, the lattice index, in the left cingulum of AD patients [21]. Although studies on autopsy brains and MR imaging have reported that the earliest changes in AD appear in the hippocampus and the olfactory cortex [7,25], recent studies using positron emission tomography (PET) [17] and single photon emission computed tomography (SPECT) suggested that the earliest changes appear in the posterior cingulate cortex rather than in the hippocampus. One possible explanation for the difference in results between morphological and functional studies is that a reduction in regional cerebral blood flow and glucose metabolism might reflect synaptic density and activity of axons projecting from other brain regions, rather than the activity of neurons in the region observed. The findings of diffusion anisotropy studies accord with those of PET and SPECT and have important implications for understanding the functional impairments of AD, because the cingulate bundles are closely related to the hippocampus and parahippocampus and are activated by attention- and memory-related tasks in humans [24] and experimental animals [9]. In conclusion, the present diffusion anisotropy study using 3.0 Tesla MR imaging showed that white matter fiber tracts were selectively affected in the temporal subcortical area, posterior corpus callosum, and cingulum in AD cases with no or only mild white matter changes in conventional MR imaging. These findings could be closely related to selective degeneration of the cerebral cortices.

The authors are grateful for the technical support of Yoshiyuki Kanbara, High Field Magnetic Resonance Imaging Research Institute, Advanced Medical Science Research Center (Iwate Medical University). This study was supported in part by a Grant-in-Aid for Advanced Medical Science Research from the Ministry of Science, Education, Sports and Culture, Japan.

[1] Arnold, S.E., Hyman, B.T., Flory, J., Damasio, A.R. and Van Hoesen, G.W., The topographical and neuroanatomical distribution of neurofibrillary tangles and neuritic plaques in the cerebral cortex of patients with Alzheimer's disease, Cereb. Cortex, 1 (1991) 103–116.
[2] Basser, P.J. and Pierpaoli, C., Microstructural and physiological features of tissues elucidated by quantitative-diffusion-tensor MRI, J. Magn. Reson., Ser. B, 111 (1996) 209–219.
[3] Beaulieu, C. and Allen, P.S., Determinants of anisotropic water diffusion in nerves, Magn. Reson. Med., 31 (1994) 394–400.
[4] Biegon, A., Eberling, J.L., Richardson, B.C., Roos, M.S., Wong, S.T., Reed, B.R. and Jagust, W.J., Human corpus callosum in aging and Alzheimer's disease: a magnetic

resonance imaging study, Neurobiol. Aging, 15 (1994) 393–397.
[5] Bozzali, M., Franceschi, M., Falini, A., Pontesilli, S., Cercignani, M., Magnani, G., Scotti, G. and Filippi, M., Quantification of tissue damage in AD using diffusion tensor and magnetization transfer MRI, Neurology, 57 (2001) 1135–1137.
[6] Bozzao, A., Floris, R., Baviera, M.E., Apruzzese, A. and Simonetti, G., Diffusion and perfusion MR imaging in cases of Alzheimer's disease: correlations with cortical atrophy and lesion load, Am. J. Neuroradiol., 22 (2001) 1030–1036.
[7] Braak, H. and Braak, E., Neuropathological staging of Alzheimer-related changes, Acta Neuropathol., 82 (1991) 239–259.
[8] Brun, A. and Englund, E., A white matter disorder in dementia of the Alzheimer type: a pathoanatomical study, Ann. Neurol., 19 (1986) 253–662.
[9] Dodart, J.C., Mathis, C., Bales, K.R., Paul, S.M. and Ungerer, A., Early regional cerebral glucose hypometabolism in transgenic mice overexpressing the V717F beta-amyloid precursor protein, Neurosci. Lett., 277 (1999) 49–52.
[10] Erkinjuntti, T., Ketonen, L., Sulkava, R., Sipponen, J., Vuorialho, M. and Iivanainen, M., Do white matter changes on MRI and CT differentiate vascular dementia from Alzheimer's disease? J. Neurol., Neurosurg., Psychiatry, 50 (1987) 37–42.
[11] Fazekas, F., Chawluk, J.B., Alavi, A., Hurtig, H.I. and Zimmerman, R.A., MR signal abnormalities at 1.5 T in Alzheimer's dementia and normal aging, Am. J. Roentgenol., 149 (1987) 351–356.
[12] Folstein, M.F., Folstein, S.E. and McHugh, P.R., "Mini-mental state", a practical method for grading the cognitive state of patients for the clinician, J. Psychiatr. Res., 12 (1975) 189–198.
[13] Hachinski, V.C., Potter, P. and Merskey, H., Leuko-araiosis, Arch. Neurol., 44 (1987) 21–23.
[14] Hanyu, H., Asano, T., Sakurai, H., Imon, Y., Iwamoto, T., Takasaki, M., Shindo, H. and Abe, K., Diffusion-weighted and magnetization transfer imaging of the corpus callosum in Alzheimer's disease, J. Neurol. Sci., 167 (1999) 37–44.
[15] Hof, P.R., Cox, K. and Morrison, J.H., Quantitative analysis of a vulnerable subset of pyramidal neurons in Alzheimer's disease: I, superior frontal and inferior temporal cortex, J. Comp. Neurol., 301 (1990) 44–54.
[16] McKhann, G., Drachman, D., Folstein, M., Katzman, R., Price, D. and Stadlan, E.M., Clinical diagnosis of Alzheimer's disease: report of the NINCDS-ADRDA Work Group under the auspices of Department of Health and Human Services Task Force on Alzheimer's Disease, Neurology, 34 (1984) 939–944.
[17] Minoshima, S., Giordani, B., Berent, S., Frey, K.A., Foster, N.L. and Kuhl, D.E., Metabolic reduction in the posterior cingulate cortex in very early Alzheimer's disease, Ann. Neurol., 42 (1997) 85–94.
[18] Pearson, R.C., Esiri, M.M., Hiorns, R.W., Wilcock, G.K. and Powell, T.P., Anatomical correlates of the distribution of the pathological changes in the neocortex in Alzheimer disease, Proc. Natl. Acad. Sci. USA, 82 (1985) 4531–4534.
[19] Reisberg, B., Ferris, S.H., de Leon, M.J. and Crook, T., The Global Deterioration Scale for assessment of primary degenerative dementia, Am. J. Psychiatry, 139 (1982) 1136–1139.
[20] Rogers, J. and Morrison, J.H., Quantitative morphology and regional and laminar distributions of senile plaques in Alzheimer's disease, J. Neurosci., 5 (1985) 2801–2808.
[21] Rose, S.E., Chen, F., Chalk, J.B., Zelaya, F.O., Strugnell, W.E., Benson, M., Semple, J. and Doddrell, D.M., Loss of connectivity in Alzheimer's disease: an evaluation of white matter tract integrity with colour coded MR diffusion tensor imaging, J. Neurol. Neurosurg. Psychiatry, 69 (2000) 528–530.
[22] Stejskal, E.O. and Tanner, J.E., Spin diffusion measurements: spin-echo in presence of a time dependent field gradient, J. Chem. Phys., 42 (1965) 288–292.
[23] Van Hoesen, G. and Damasio, A., Neuronal correlates of cognitive impairment in Alzheimers disease, In V.B. Mountcastle, F. Plum and S.R. Geiger (Eds.), The Handbook of Physiology, Vol. 5, American Physiology Society, Baltimore, MD, 1987, pp. 871–898.
[24] Vogt, B.A., Finch, D.M. and Olson, C.R., Functional heterogeneity in cingulate cortex: the anterior executive and posterior evaluative regions, Cereb. Cortex, 2 (1992) 435–443.
[25] Xu, Y., Jack Jr, C.R., O'Brien, P.C., Kokmen, E., Smith, G.E., Ivnik, R.J., Boeve, B.F., Tangalos, R.G. and Petersen, R.C., Usefulness of MRI measures of entorhinal cortex versus hippocampus in AD, Neurology, 54 (2000) 1760–1767.
[26] Yamanouchi, H., Sugiura, S. and Shimada, H., Decrease of nerve fibers in the anterior corpus callosum of senile dementia of Alzheimer type, J. Neurol., 236 (1989) 491–492.
[27] Yamauchi, H., Fukuyama, H., Harada, K., Nabatame, H., Ogawa, M., Ouchi, Y., Kimura, J. and Konishi, J., Callosal atrophy parallels decreased cortical oxygen metabolism and neuropsychological impairment in Alzheimer's disease, Arch. Neurol., 50 (1993) 1070–1074.

ELSEVIER

Molecular Brain Research 106 (2002) 88–93

MOLECULAR BRAIN RESEARCH

www.elsevier.com/locate/bres

Research report

# Over-expression of α7 nicotinic acetylcholine receptor induces sustained ERK phosphorylation and *N*-cadherin expression in PC12 cells

Kimiaki Utsugisawa, Yuriko Nagane, Daiji Obara, Hideo Tohgi*

*Department of Neurology, Iwate Medical University, Uchimaru 19-1, Morioka 020 Japan*

Accepted 1 August 2002

**Abstract**

Over-expression of α7 nicotinic acetylcholine receptor (α7nAChR) in PC12 cells, independent of agonistic stimulation, induces marked neurite outgrowth and high capacity for migration and adherence (differentiation-like transformation), and increases tolerance against cell damage. In the present study, we investigated the effects of α7nAChR over-expression and nicotine on ERK phosphorylation and *N*-cadherin expression by comparing 3 groups of cells: PC12 cells transfected with α7 subunit cDNA (α7pCMV cells); untransfected PC12 cells exposed to 50 μM nicotine (PC12 cells+nicotine); and PC12 cells transfected with vector only (pCMV cells). α7 subunit protein was detected in α7pCMV cells at 24 to 72 h after transfection. α7pCMV cells exhibited sustained expression of phospho-ERKs (p42 and p44) at 24 to 72 h after transfection, and differentiation-like transformation at 72 h after transfection. PC12 cells+nicotine exhibited transient expression of phospho-ERKs at 48 h after addition of nicotine, but did not exhibit differentiation-like transformation. Neither ERK phosphorylation nor differentiation-like transformation was observed in pCMV cells. Expression of surface *N*-cadherin increased at 72 h after transfection on α7pCMV cells, but did not increase on PC12 cells+nicotine or pCMV cells. These findings suggest that, in PC12 cells, over-expression of α7nAChR induces sustained activation of ERK, which probably promotes *N*-cadherin expression and differentiation-like transformation.


*Theme:* Neurotransmitters, modulators, transporters, and receptors

*Topic:* Acetylcholine receptors: nicotinic

*Keywords:* Differentiation; ERK; *N*-cadherin; Neurite outgrowth; α7 nicotinic acetylcholine receptor

## 1. Introduction

The α7 subtype of neuronal nicotinic acetylcholine receptor (α7nAChR) forms homomeric ion channels that efficiently promote $Ca^{2+}$ influx and are rapidly desensitized [7,29]. α7nAChR has been found to be expressed throughout the mammalian brain [4,29], and is assumed to modulate synaptic transmission [14,19] and the plasticity of neuronal circuitry [2,5–7]. Notably, α7nAChR exerts neuroprotective effects against various types of cell damage due to glutamate-, arachidonic-acid- and β amyloid-induced cytotoxicity and hypoxia in vitro [1,9,11,13,17,26]. The neuroprotective effects of nicotine via α7 nAChR have been assumed to be due to $Ca^{2+}$-buffering mechanisms [7] such as agonist-mediated quick $Ca^{2+}$ currents via α7 nAChR. It has also been reported that phosphatidylinositol 3-kinase (PI3-K) mediates neuroprotective functions of nicotine via α7 nAChR [17], suggesting that α7 nAChR can affect neuroprotective signaling systems. Furthermore, in our most recent study, α7nAChR over-expression, independent of agonistic stimulation, prevented G1-arrest of the cell cycle and DNA fragmentation induced by hypoxia in PC12 cells (a rat pheochromocytoma cell line) [27]. PC12 cells over-ex-

*Abbreviations*: DMEM, Dulbecco's modified Eagle's medium; EGF, epidermal growth factor; ERK, extracellular-signal-regulated kinase; FGF, fibroblast growth factor; MAPK, mitogen-activated protein kinases; nAChR, nicotinic acetylcholine receptor; NGF, nerve growth factor; PC12, rat pheochromocytoma cells; PI3-K, phosphatidylinositol 3-kinase

*Corresponding author. Tel.: +81-19-651-5111; fax: +81-19-654-9860.

*E-mail address:* htohgi@iwate-med.ac.jp (H. Tohgi).

0169-328X/02/$ – see front matter 
PII: S0169-328X(02)00415-1

pressing α7nAChR exhibited marked neurite outgrowth and high capacity for migration and adherence (differentiation-like transformation), along with an increase in expression of Akt, which functions down-stream of PI3-K and keeps neurons alive [27]. However, the mechanisms underlying the differentiation-like transformation induced by α7nAChR over-expression have not been determined.

PC12 cells have been used extensively as a model system to study the signaling elements that initiate neurite outgrowth and differentiation [10,16,18], which occur in response to nerve growth factor (NGF) or basic fibroblast growth factor (bFGF). Treatment of PC12 cells with NGF triggers differentiation into sympathetic neuron-like cells that exhibit neurite outgrowth, and induces sustained activation of extracellular-signal-regulated kinase (ERK), a member of the mitogen-activated protein kinase (MAPK) family [18]. ERK, also known as classical MAPK, is activated in response to various growth and differentiation factors, and plays a significant role in differentiation and early embryonic development [10,18]. *N*-cadherin has also been shown to be essential for neurite outgrowth in vitro [10,12,28]. *N*-cadherin can activate ERK and induces neurite outgrowth [22,23]. Therefore, we investigated the effects of α7nAChR over-expression and nicotine on ERK phosphorylation and *N*-cadherin expression in PC12 cells.

## 2. Materials and methods

### 2.1. Cell culture and plasmids

Preparation of α7 subunit cDNA and plasmids was performed as previously described [27]. A PC12 cell line [15] (JCRB 0733; Human Science Research Resource Bank, Osaka, Japan) was maintained in Dulbecco's modified Eagle's medium (DMEM) supplemented with 10% fetal bovine serum (FBS), 100 units/ml penicillin, and 100 μg/ml streptomycin in a humidified atmosphere containing 5% $CO_2$ at 37°C, without trypsin-EDTA for cell subculture. Three groups of PC12 cells were designated: PC12 cells transfected with α7 subunit cDNA inserted in C-terminal-FLAG-tagging pCMV vector (STRATAGENE) (α7pCMV cells); untransfected PC12 cells exposed to 50 μM nicotine (PC12 cells+nicotine); PC12 cells transfected with pCMV vector only (without α7 subunit cDNA) (pCMV cells). PC12 cells were transfected with α7pCMV or pCMV plasmid by lipofection using Effectene™ Transfection Reagent (QIAGEN). Cells were harvested for subsequent analysis at 24, 48 and 72 h after transfection or addition of nicotine to the medium. A subset of α7pCMV cells was treated with 0.75 mg/ml G418 (Calbiochem) for 3 days. After removal of G418, the surviving cells were maintained for an additional 4 days in order to select stable integrants (α7 stably-expressing cells) [27]. Our recent study has demonstrated that α7 subunit proteins coded for by the transfected α7 cDNA formed functional complexes and were expressed on the membranes of the α7pCMV cells [27].

### 2.2. Immunoblotting for ERKs and other MAPKs

Cell lysates were prepared in lysis buffer (50 mM HEPES, 1 mM EDTA, 150 mM NaCl, pH 7.5) containing 1% NP40, 1 mM sodium orthovanabate (SV), 1 mM dithiothreitol (DTT), 10 mM NaF and Protein Inhibitor Cocktail (CALBIOCHEM). Proteins were subjected to electrophoresis in SDS–8% polyacrylamide gel, and then transferred electrophoretically to nitrocellulose membranes (Schleicher and Schuell). The membranes were blocked with 5% dried milk/tris-buffered saline (pH 7.4) with 0.1% Tween 20 (TTBS), and were incubated with primary antibodies diluted 1:1000 for 1 h at room temperature. After washing with TTBS, the membranes were incubated with horseradish peroxidase-conjugated anti-mouse (Amersham) or anti-rabbit IgG (Amersham) diluted 1:3000, and then washed with TTBS. Detection was performed using an enhanced chemiluminescence (ECL) system (NEN). The chemiluminescence signals from the CCD camera were integrated for 20 s into the computer memory directly from the membranes using the Chemi Doc system (BIO-RAD). Primary antibodies used were anti-p44- and p42-MAPKs (ERKs) (Cell Signaling Technology), anti-c-Jun-N-terminal kinase (JNK)-1 (Santa Cruz), anti-p38 MAPK (Transduction Laboratories), anti-phospho- p44- and p42-MAPKs (ERKs) (Cell Signaling Technology), anti-phospho-SAPK/JNK (Cell Signaling Technology), anti-phospho-p38 MAPK (Cell Signaling Technology), anti-FLAG (SIGMA) and anti-actin (PROGEN).

### 2.3. Flow cytometry for estimation of N-cadherin expression

Cells were immediately washed with cooled phosphate-buffered saline (PBS), semi-fixed with 70% ethanol in PBS, and incubated with anti-*N*-cadherin (extracellular domain) antibodies (Santa Cruz) diluted 1:50 for 1 h at 4°C. After washing with PBS, the cells were incubated with RPE-conjugated anti-rabbit IgG (ICN Biomedicals) diluted 1:100, then washed with PBS, and monitored for surface *N*-cadherin expression by FACScan. Analysis was performed for $5\times10^4$ cells.

## 3. Results

### 3.1. Morphological changes in PC12 cells due to α7 over-expression

α7pCMV cells underwent a differentiation-like transformation. At 72 h after transfection, they exhibited marked neurite outgrowth and high capacity for migration and adherence to the culture dish (Fig. 1b), compared with